Available online at www.sciencedirect.com
ScienceDirect
Ceramics International 37 (2011) 3599–3608
CERAMICS INTERNATIONAL
www.elsevier.com/locate/ceramint

Influence of small amount of sintering additives on unlubricated sliding wear properties of SiC ceramics

B.V. Manoj Kumar [a], Young-Wook Kim [a,*], Dae-Soon Lim [b], Won-Seon Seo [c]

[a] Functional Ceramics Laboratory, Department of Materials Science and Engineering, University of Seoul, Seoul 130-743, Republic of Korea
[b] Department of Materials Science and Engineering, Korea University, Seoul 136-701, Republic of Korea
[c] Korea Institute of Ceramic Engineering and Technology, Seoul 153-801, Republic of Korea

Received 1 February 2011; received in revised form 1 June 2011; accepted 9 June 2011
Available online 15 June 2011

Abstract

Fully densified SiC ceramics were developed from commercially available β-SiC powders using small amount (3 wt%) of AlN–Sc_2O_3 or AlN–Y_2O_3 additives by hot pressing at 2050 °C for 6 h in nitrogen atmosphere, and their wear properties were investigated by subjecting to self-mated sliding at different loads (1, 6 and 13 N) under unlubricated conditions. SiC ceramics prepared with 3 wt% AlN–Y_2O_3 additives consisted of mostly large equi-axed grains with amorphous grain boundary phase of ~1.2 nm thickness, whereas SiC ceramics sintered with 3 wt% AlN–Sc_2O_3 additives showed duplex microstructure of elongated and fine equi-axed grains with clean grain boundary. As the load was increased, the steady state coefficient of friction reduced from ~0.6 to ~0.2, and wear rate increased from 10^{-6} to 10^{-5} $mm^3/N{\cdot}m$. It was observed that the friction did not depend on the additive composition, while less wear was observed for the SiC ceramics sintered with 3 wt% AlN–Sc_2O_3 additives consisting of clean grain boundary. The material loss was increased with the increased amount of sintering additive to 10 wt%. The worn surface morphology revealed that the material was primarily removed via surface grooving and microcracking at 1 N load, while tribochemical wear dominated at 6 and 13 N loads.

Keywords: Silicon carbide; Sintering additives; Sliding wear

1. Introduction

Silicon carbide is considered as a suitable material for various structural applications such as mechanical seals, bearings and cylinder liners because of its superior properties of high hardness, high temperature strength and excellent resistance to wear and corrosion [1–3]. Accordingly, extensive research has been carried out towards estimating the tribological potential of this important material in various conditions [4–17]. The coefficient of friction (COF) in the reported sliding studies varied in the wide range of 0.2–0.8, while wear rates were in the order of 10^{-7} to 10^{-5} $mm^3/N{\cdot}m$. [5–9]. The complex wear behavior was largely explained by several mechanisms of material removal such as plastic deformation, ploughing, and/or formation and removal of tribooxide layer [5–14]. While most of the published research about sliding wear of SiC ceramics was conducted to estimate the influence of sliding test, material or environmental parameters, the influence of microstructural characteristics on unlubricated sliding wear behavior is relatively less reported. Cho et al. [13] and Lopez et al. [14–16] studied the effect of microstructure on sliding wear properties of SiC ceramics under paraffin oil lubrication and reported that wear resistance decreased with an increase in the content of intergranular phase, grain coarsening or applied load.

The liquid-phase sintering using metal oxides, Al-B-C, AlN–metal oxides as sintering additives is recommended for producing SiC ceramics with tailored microstructure and improved fracture toughness [17–20]. Among various additive systems, AlN and RE_2O_3 (RE: rare-earth elements) system is preferred due to relatively less weight loss [21], easy control of oxynitride decomposition and absence of gas phase reactions below 2000 °C [18]. The use of RE_2O_3 renders SiC ceramics with excellent high temperature strength and toughness properties [22]. The platelet-reinforced microstructures exhibit enhanced toughness due to the combination of

* Corresponding author. Tel.: +82 2 2210 2760.
E-mail address: ywkim@uos.ac.kr (Y.-W. Kim).

0272-8842/$36.00
doi:10.1016/j.ceramint.2011.06.018

intergranular crack mode, introduced by the glassy grain boundary phase, and energy dissipating processes in the crack wake [23]. It has been recently identified that sintering additive composition plays a dominant role in effecting the crystallinity of grain boundary phase. Amorphous intergranular phase was obtained using AlN–Y_2O_3 [24,25] and AlN–Er_2O_3 [19] additives systems, whereas AlN–Sc_2O_3 render clean grain boundary [26,27], and AlN–Lu_2O_3 systems render clean [28] or crystallized grain boundary [29]. It is to note that most of the published research was conducted towards characterization of SiC ceramics prepared with relatively large amounts (≥5 wt%) of sintering additives, while processing and properties of SiC ceramics sintered with small amount of additives was rarely reported [30]. In order to achieve conceptual advancement in the design of wear-resistant ceramics, it becomes necessary to understand the influence of small amount of sintering additives on unlubricated sliding wear properties of SiC ceramics.

In this context, SiC ceramics consisting of different microstructural characteristics were fabricated using small amount (3 wt%) of AlN–RE_2O_3 (RE: Y and Sc) additives in the present study, and the particular influence of additive composition on the sliding wear properties under unlubricated conditions was discussed.

2. Experimental

Commercially available β-SiC (Ultrafine grade, Betarundum, Ibiden Co. Ltd., Ogaki, Japan), AlN (Grade F, Tokuyama Soda Co., Tokyo, Japan), and metal oxides (Y_2O_3, and Sc_2O_3, 99.9% pure, Shin-Etsu Chemical Co., Tokyo, Japan) were used as the starting powders. The mean particle size and the specific surface area of the β-SiC powders were 0.27 μm and 17.5 m^2/g, respectively. A powder mixture of SiC and 3 wt% additives, AlN and RE_2O_3 (RE: Y, Sc) was prepared. The relative amount of RE_2O_3 in the total content of additives was 20 mol%. The respective powder batches were milled in ethanol for 24 h using SiC grinding balls. The milled slurry was dried, sieved, and hot-pressed at 2050 °C for 6 h under a pressure of 25 MPa in N_2 atmosphere. For comparison, ceramics with initial powder mixture of SiC and 10 wt% AlN–Sc_2O_3 were also prepared. The details of specimen designation, batch composition and additive systems are given in Table 1.

The bulk density of the sintered specimen was measured using the Archimedes method. The theoretical densities of each specimen were calculated according to the rule of mixtures using the following densities: β-SiC 3.216 g/cm^3 (JC-PDF #29-1129), AlN 3.261 g/cm^3 (JC-PDF #25-1133), Y_2O_3 5.032 g/cm^3 (JC-PDF #43-1036), and Sc_2O_3 3.840 g/cm^3 (JC-PDF #43-1028). The sintered specimens were cut in the perpendicular direction to pressing axis, polished, and etched using a CF_4 plasma containing 20% O_2. The grain morphology was observed using scanning electron microscopy (SEM, S4300, Hitachi Ltd., Japan). After regular methods of sample preparation, high resolution transmission electron microscopy (HRTEM, 400 kV, JEM-4010, JEOL, Japan) was used to observe SiC–SiC and SiC-junction phase boundaries and to determine the presence of amorphous phases at the grain boundaries. The chemical compositions of the grains and junctions were analyzed by using energy dispersive spectroscopy (EDS). A scanning TEM interface box was integrated with the microscope so that an electron probe of 15 nm diameter could be used for the EDS analysis of grains and ternary junctions. The microhardness and macrohardness of the polished specimens were measured by Vickers indentation, done at 2.9 N load for dwell time of 10 s (MVK-H1, Akashi Corporation, Japan) and 196 N load for dwell time of 30 s (AVK-C2, Akashi Corporation, Japan), respectively. The lengths of cracks generated by Vickers indentation at 196 N were measured and fracture toughness was estimated using the following formula [31].

$$K_{I_c} = 0.016\left(\frac{E}{H}\right)^{0.5}\frac{P}{c^{1.5}} \quad (1)$$

where H is hardness, P is load, and c is crack length. Elastic modulus E of 443 GPa was used.

Wear tests were conducted on polished bar shaped SiC sintered specimens of 5 mm × 15 mm × 15 mm size against commercial SiC balls (hardness: 25–28 GPa, surface roughness: Ra 8 nm, SBB Tech. Co., Suwon, Korea) of 6.35 mm diameter using a unidirectional ball-on-disk tribometer in ambient conditions (20 ± 5 °C and 50 ± 10% RH). The detailed description of the tribometer can be found elsewhere [32]. Both SiC balls and sintered SiC disks were ultrasonically cleaned with acetone prior to wear testing. SiC balls were fixed in the ball holder so as to make a track radius of 2.0 mm from the central axis and the tests were conducted at a fixed rotational speed of 1000 rpm (linear speed of 0.21 m/s) for 15 min (total sliding distance of 188 m). The sliding tests were carried out at 1 N, 6 N or 13 N load that resulted in a maximum Hertzian contact stress (initial) of 1.1, 1.9 or 2.5 GPa, respectively. During the test runs, frictional forces were recorded using an electronic sensor to generate real time coefficient of friction (COF) data. Surface profiles of the worn disk specimens were

Table 1
Batch composition, and physical and mechanical properties of sintered SiC specimens.

Specimen designation	Batch composition (wt%)	Additive content (wt%)	Relative density (%)	Hardness (GPa)		Fracture Toughness ($MPa{\cdot}m^{1/2}$)
				$HV_{0.3}$	HV_{20}	
SCY3	97 β-SiC + 1.262 AlN + 1.738 Y_2O_3	3	98.0	21.4 ± 3.3	19.2 ± 2.7	4.1 ± 1.3
SCSc3	97 β-SiC + 1.629 AlN + 1.371 Sc_2O_3	3	99.2	26.2 ± 3.3	23.3 ± 4.0	6.4 ± 0.8
SCSc10	90 β-SiC + 5.430 AlN + 4.570 Sc_2O_3	10	99.9	24.7 ± 0.0	22.0 ± 1.3	3.4 ± 0.1

acquired using an alpha-step profilometer (Model No.: 500, TENCOR, Germany) to measure the depth and width of wear tracks. The wear track width and maximum depth were further used in computing the wear volume (and subsequently wear rate) of the SiC disk specimens according to following relations.

$$V = 2\pi rwd \tag{2}$$

$$WR = \frac{V}{Ps} \tag{3}$$

where V is wear volume (mm^3); r, w and d are radius, width and depth of wear track, respectively (mm); P is normal load (N); s is total sliding distance (m); WR is the wear rate in (mm^3/N·m). In order to understand the wear mechanism, a detailed microstructural characterization of the as-worn surfaces was conducted using SEM.

3. Results and discussion

The influence of additive composition on density of the sintered SiC specimen is shown in Table 1. The hot pressing of the investigated powder mixtures resulted in high density (≥98%). During hot-pressing, AlN–RE_2O_3 additives react with the native SiO_2, present on SiC particles to form an RE–Si–Al–oxynitride melt, which upon heating to high temperature forms RE–Si–Al–O–C–N melt by dissolution of SiC [27–29]. Thus, solution-reprecipitation occurring during liquid phase sintering (LPS) promotes densification. The present results essentially indicate that small amount (3 wt%) of sintering additives used was sufficient for the densification of Sc_2O_3 or Y_2O_3-containing additive systems.

The representative microstructures of the plasma-etched surfaces of the sintered specimens are provided in Fig. 1. In general, all specimens showed microstructures consisting of platelet α-SiC (elongated, in two dimensions) and equi-axed β-SiC grains. The microstructure of SCY3 consisted of equi-axed and platelet grain structure (Fig. 1a), whereas that of SCSc3 showed thick and largely elongated, and fine equi-axed grains (Fig. 1b). With increased additive content to 10 wt%, the SCSc10 showed limited grain growth (Fig. 1c). Further, it was understood that the cations of additives incorporated into the RE–Al–Si–oxycarbonitride glass phase effectively alter the physical properties, force balance and, in turn, the thickness of the intergranular film [33]. Typical TEM images of junction phase and grain boundaries of the sintered specimen are shown in Fig. 2. EDS analysis at the SiC–SiC junctions showed the presence of secondary phases, such as Y–O–Si–C in SCY3 (Fig. 2a). Furthermore, HRTEM images in Fig. 2b and c reveal that SCY3 microstructure contained an amorphous grain boundary phase of ∼1.2 nm thickness, whereas clean grain boundary is observed in SCSc specimen. Thus, the smaller cation appears to lead the higher tendency for the clean boundaries. These results are consistent with the reported TEM studies of systems with 10 vol% AlN–RE_2O_3 (RE: Sc, Y, Lu) additives [26–28].

The surface morphology of the fractured SiC ceramics is shown in Fig. 3. All specimens in general exhibit mixed characteristics of transgranular and intergranular fracture. The large elongated grains in SCSc3 indicate more tortuous crack

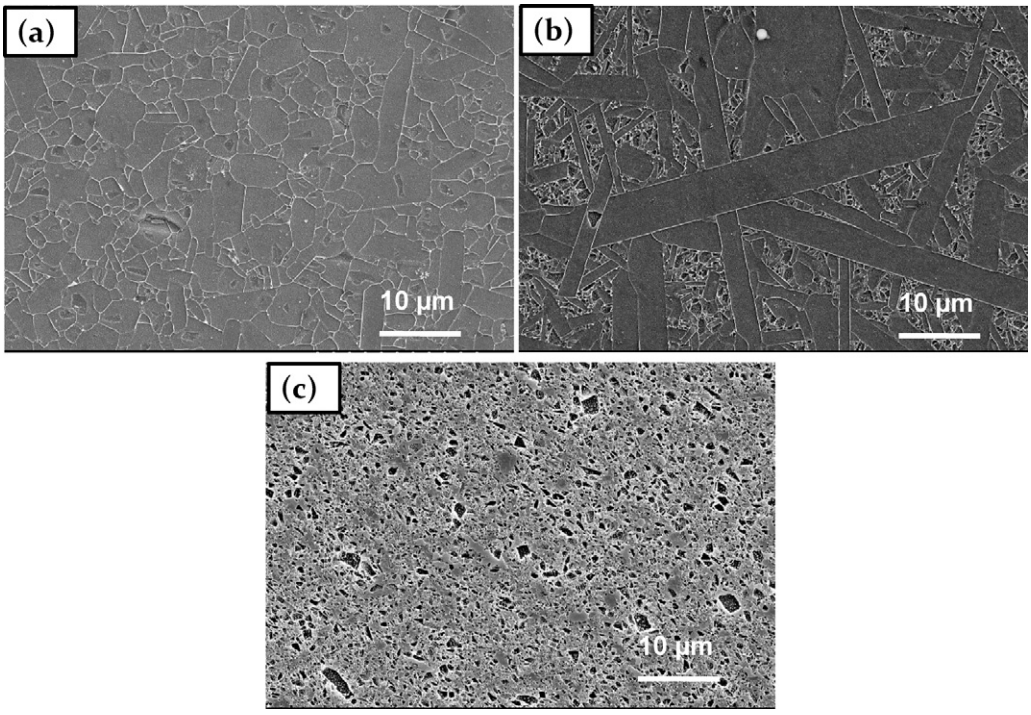

Fig. 1. Representative microstructures of polished and etched surfaces of developed SiC ceramics (a) SCY3, (b) SCSc3, and (c) SCSc10. Refer Table 1 for sample designation.

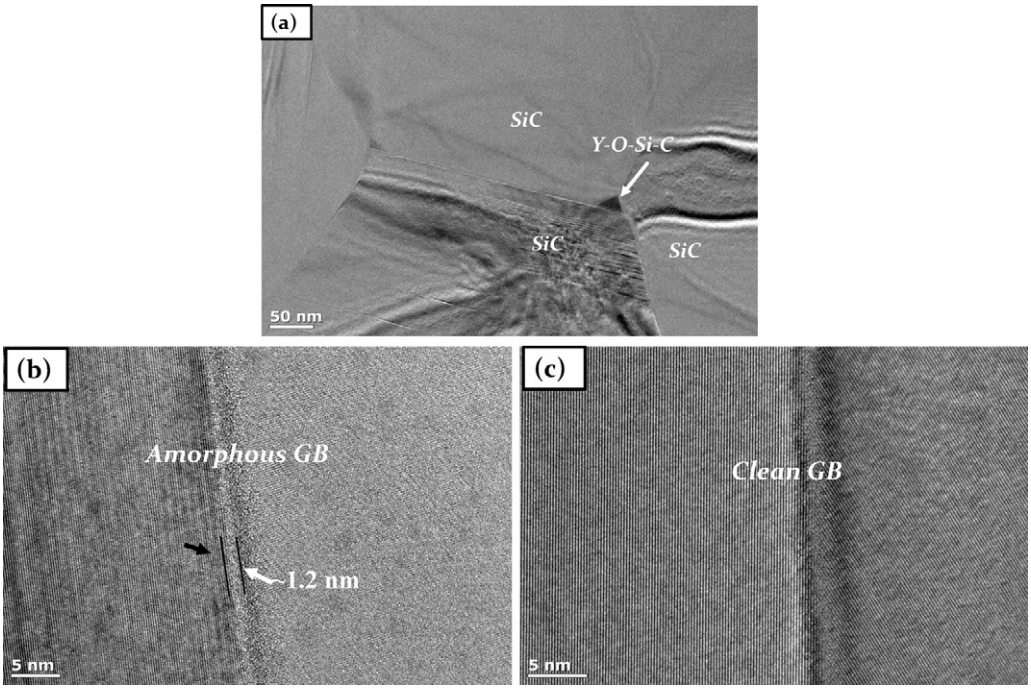

Fig. 2. TEM images of SiC ceramics revealing (a) junction phases in SCY3, (b) amorphous grain boundary in SCY3, and (c) clean grain boundary in SCSc3.

path that may lead to higher fracture toughness. Usually, crack bridging, frictional grain bridges, and elastic bridges are reported as major toughening mechanisms for the LPS-SiC ceramics [34,35]. Several investigations suggest that the variation in the composition of the sintering additives and hence the composition of the grain boundary phase can play a significant role in altering the crack propagation behavior of LPS-SiC ceramics [36,37]. Similar observations were reported for SiC ceramics sintered with $Y_3Al_5O_{12}$ and SiO_2 [36] and SiC ceramics sintered with RE_2O_3 (RE: La, Y, Nd, Yb) and Al_2O_3 [37].

The hardness and facture toughness measurements of SiC ceramics sintered with small amount of additives are presented in Table 1. A maximum micro hardness of ~26 GPa was recorded for SCSc3, while SCY3 exhibited minimum micro hardness of ~21 GPa. The presence of weak

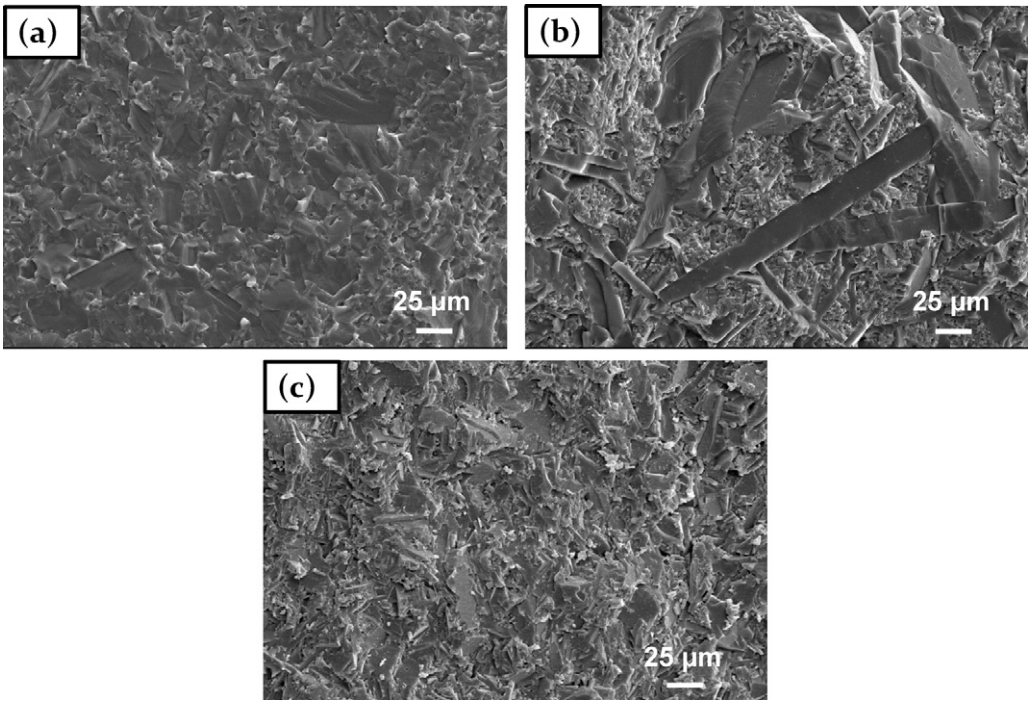

Fig. 3. Fracture surfaces of SiC ceramics: (a) SCY3, (b) SCSc3, and (c) SCSc10.

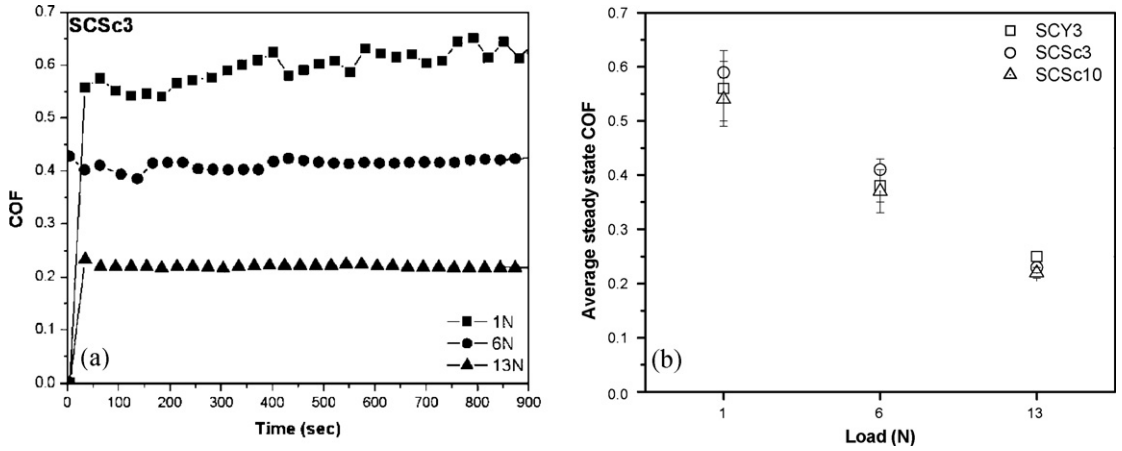

Fig. 4. (a) The evolution of coefficient of friction (COF) with time for the SCSc3 ceramics slid at different loads and (b) average COF of SiC ceramics as a function of load.

amorphous grain boundary phase resulted in low hardness for SCY3, whereas the clean grain boundary phase provided the highest hardness for SCSc3. With increased additive content, SCSc10 showed a slightly reduced hardness of ∼25 GPa, which can be attributed to the increased volume fraction of secondary phases. However, finer microstructure in SCSc10 resulted in higher hardness than that observed in SCY3. Further, macro hardness measurements were 2–3 GPa lower than their respective micro hardness values. Indeed, SCSc3 exhibited the highest hardness of ∼23 GPa amongst the investigated ceramics. It is also evident from Table 1 that SCSc3 specimen possessed the highest fracture toughness of 6.4 MPa·m$^{1/2}$, whereas SCY3 exhibited 4.1 MPa·m$^{1/2}$. With increased additive content, SCSc10 showed the lowest fracture toughness of 3.4 MPa·m$^{1/2}$. Relating to the microstructural characteristics, the high toughness of SCSc3 was attributed to the presence of large platelet grains and more tortuous fracture surface in SCSc3, while finer microstructure resulted in low toughness in SCY3 or SCSc10.

When subjected to unlubricated sliding against SiC balls, all sintered SiC specimens exhibited an almost identical evolution of COF with time regardless of the additive composition or content (Fig. 4). The general observation is that COF increased to a peak value during initial 100 s (running-in-period) and thereafter attained a steady state. With increase in load from 1 to 13 N, fluctuations reduced (Fig. 4a) and average steady state COF decreased (Fig. 4b). There existed a small difference in steady state COF with respect to additive composition at low load (1 N), while such a variation diminished at intermediate (6 N) or high (13 N) load. A maximum steady state COF of 0.56 was recorded for SCY3 at 1 N, while a minimum steady state COF of 0.22 recorded for all specimens at 13 N. The COF in the reported sliding studies varied from 0.2 to 0.6, based on the experimental and material parameters, while low COF was largely attributed to the formation of hydrated silica at the sliding interface [6–8]. Results from the present study indicate that the frictional behavior of the SiC ceramics was mostly independent of additive composition or content, while COF largely decreased with increase in load.

Typical surface profiles of the wear scar acquired in the transverse direction of sliding are shown in Fig. 5. The average width of the wear scar varied between 190 and 1200 μm, and the maximum depth up to which the material can be removed varied between 0.3 and ∼14 μm. The scar width as well as maximum depth increased with increase in load for all the specimens. SCSc3 specimen showed distinctly less damage than other specimens after sliding at 6 or 13 N load. Fig. 6 shows wear rate of the investigated SiC ceramics at different loads. The wear rate increased from 10^{-6} to 10^{-5} mm^3/N·m

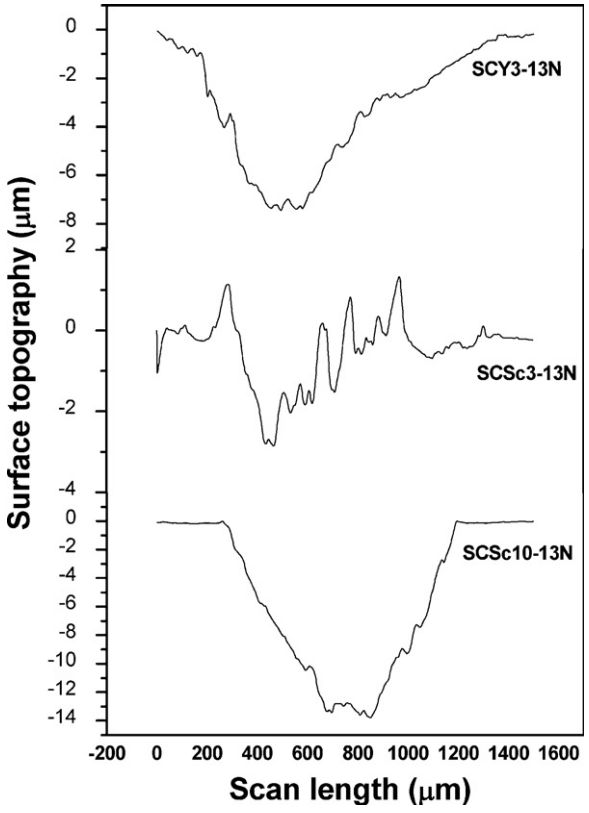

Fig. 5. Typical profiles of worn surfaces of SiC ceramics after sliding at 13 N load.

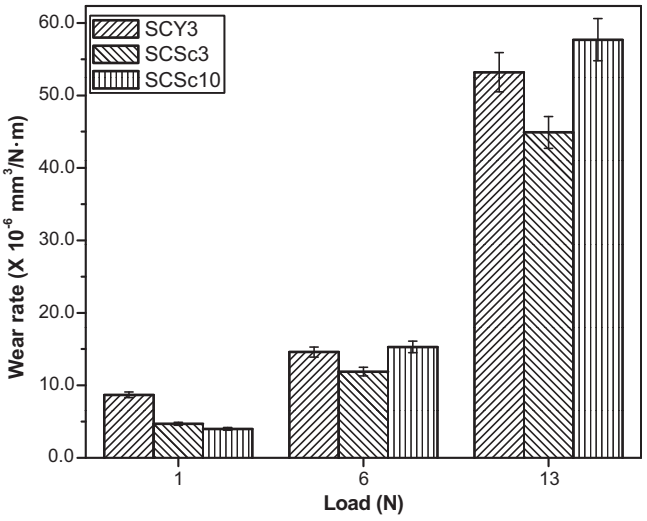

Fig. 6. Wear rate of SiC ceramic disks as a function of load.

with increase in load. SCSc3 showed less wear than SCY3 at a given load. With increase in additive content, SCSc10 showed high wear. The commonly reported wear rates for the LPS-SiC ceramics with varying experimental or environmental conditions lie in the range of 10^{-7} to 10^{-5} mm^3/N·m [8,11].

The influence of additive composition on the worn surface morphology of the investigated SiC ceramics is shown in Figs. 7–9. At low load of 1 N, worn surfaces of all specimens showed surface grooving and microfracture (Fig. 7). The compaction of debris was also observed on the worn surface of SCSc3 (Fig. 7b). The worn surface of the counterbody ball shows surface polishing (Fig. 7d). At increased load of 6 N, the worn surfaces of the specimens were mostly covered by the debris layers. Fig. 8a shows thick tribolayer containing several cracks as well as intragranular fracture of the sub-surface of SCY3. However, the tribolayer formed on SCSc3 at 6 N load (Fig. 8b) appears rather smooth and ductile with less cracking, indicating its superior load bearing capacity. On the other hand, cracking of the tribolayer is observed for SCSc10. Such a difference in the characteristics of tribolayer is essentially related to the response of the base material, as the latter affects the stress state of the material under sliding conditions. The worn surfaces in Fig. 9 show the inability of the tribolayer to bear the high load of 13 N during sliding. While, tribolayer is still present on the worn surface of SCSc3, the presence of thin layer or its removal can be noted on SCY3 or SCSc10. The observed changes in the severity of damage are consistent with the wear measurements. The wear rate was increased with load, and less for the SCSc3 specimen (Fig. 6).

The worn surfaces of the counterbody ball when slid against the SiC disks at 6 and 13 N loads are shown in Fig. 10. Insets in Fig. 10a–c illustrate small wear scar diameters for the ball worn at 6 N load against SCSc3 (585 μm) when compared against SCY3 (645 μm) or SCSc10 (670 μm). Further, the worn surfaces show tribolayer fragments at the edges and surface polishing at the centre after sliding at 6 N load. The worn surface of SCSc3 contained thin layer at the centre as well, and the SCSc10 showed number of debris and abraded grooves. Considering the dominant tribolayer formation on the worn disk surfaces (Fig. 8), it can be understood that the sliding occurred between the worn ball surface and the tribolayer on the disk surfaces. Thus, friction between tribolayer and the worn ball surface was less at 6 N load when compared to the

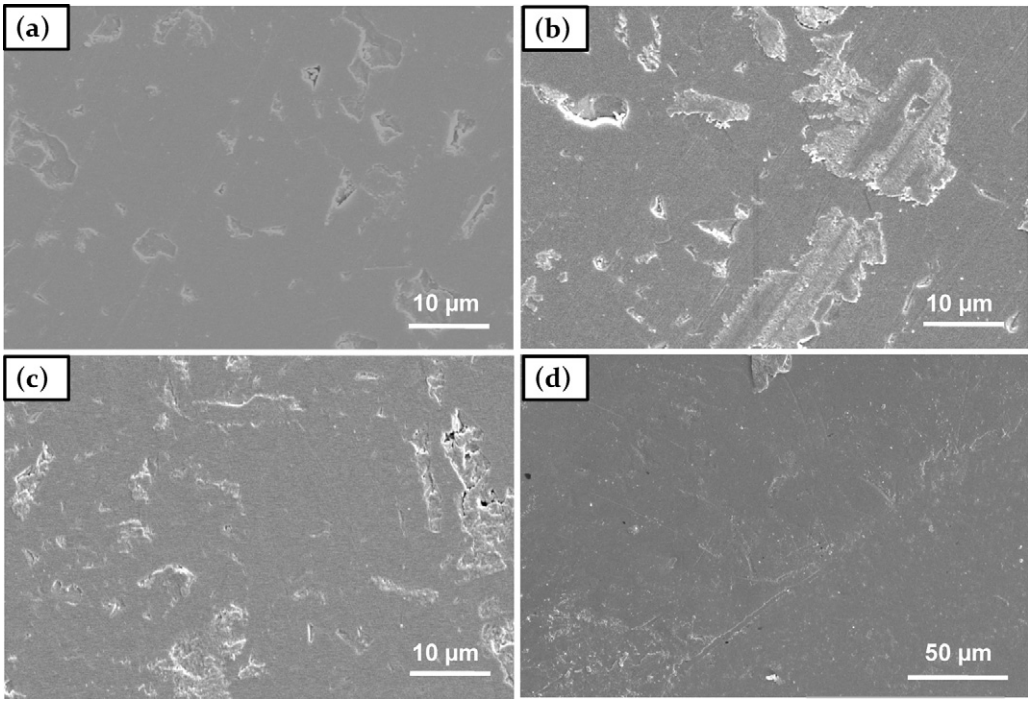

Fig. 7. Worn surface morphology of SiC ceramics after sliding at 1 N load: (a) SCY3, (b) SCSc3, and (c) SCSc10. Worn surface of ball after sliding against SCY3 at 1 N load is shown in (d).

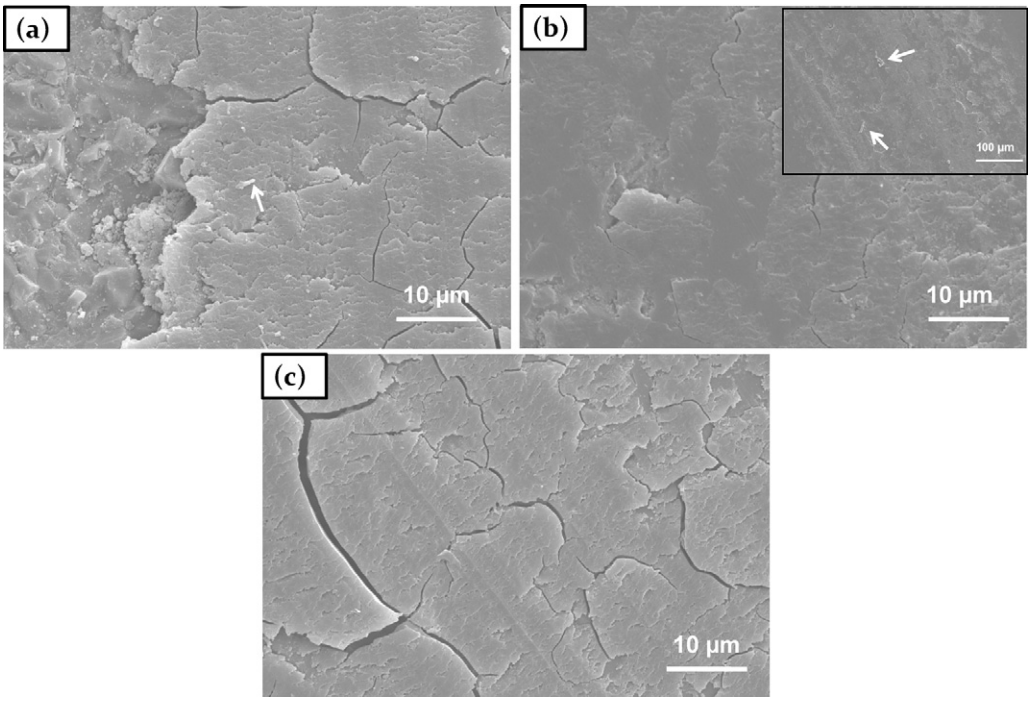

Fig. 8. Worn surface morphology of SiC ceramics after sliding at 6 N load: (a) SCY3, (b) SCSc3, and (c) SCSc10. Arrows indicate the needle-like debris particles.

friction between the worn surfaces of ball and disk at 1 N load (Fig. 4b). The tribolayer fragments observed at the edge of the ball surfaces suggests transfer of tribolayer from the disk surface. However, the worn surface of the balls slid against 13 N load is found to be covered mostly by the thick tribolayer (Fig. 10d). It is probable that such a thick tribolayer is either formed on the ball surface due to the compaction of the debris or transferred from the disk surface under high loading (13 N) conditions. This basically implies that the sliding occurred between the tribolayers at the contact. Since, the friction between the tribolayers was obviously less than the friction between the tribolayer and the worn ball surface (as observed at 6 N), lower COF values were obtained for the specimens slid at 13 N (Fig. 4b). Cylindrical debris of length and diameter

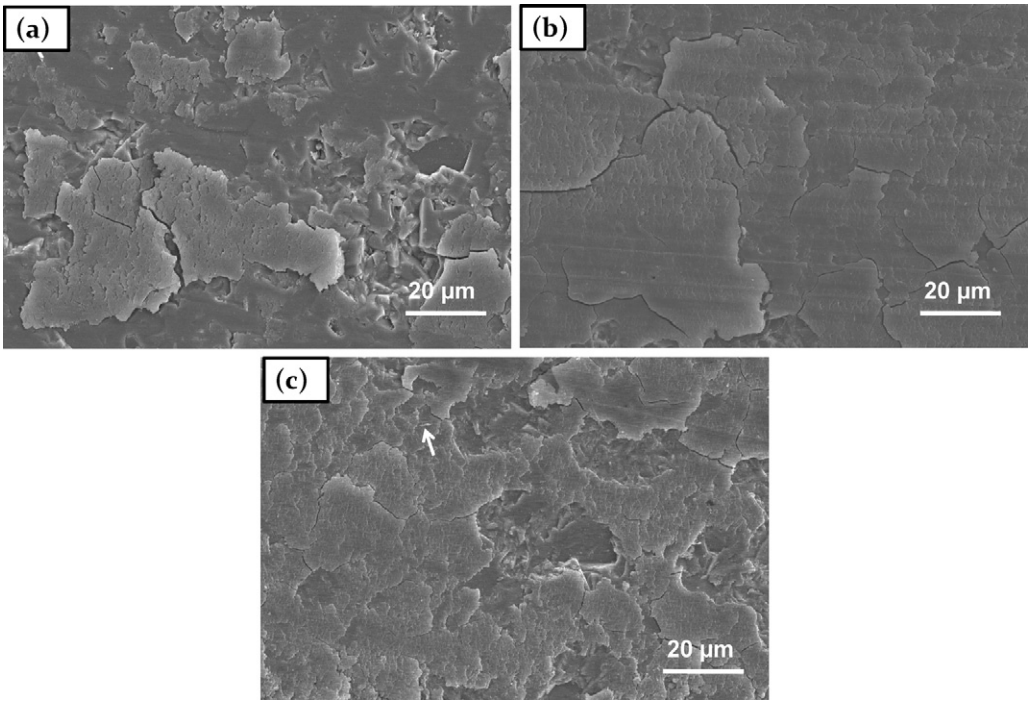

Fig. 9. Worn surface morphology of SiC ceramics after sliding at 13 N load: (a) SCY3, (b) SCSc3, and (c) SCSc10. Arrow indicates the needle-like debris particles.

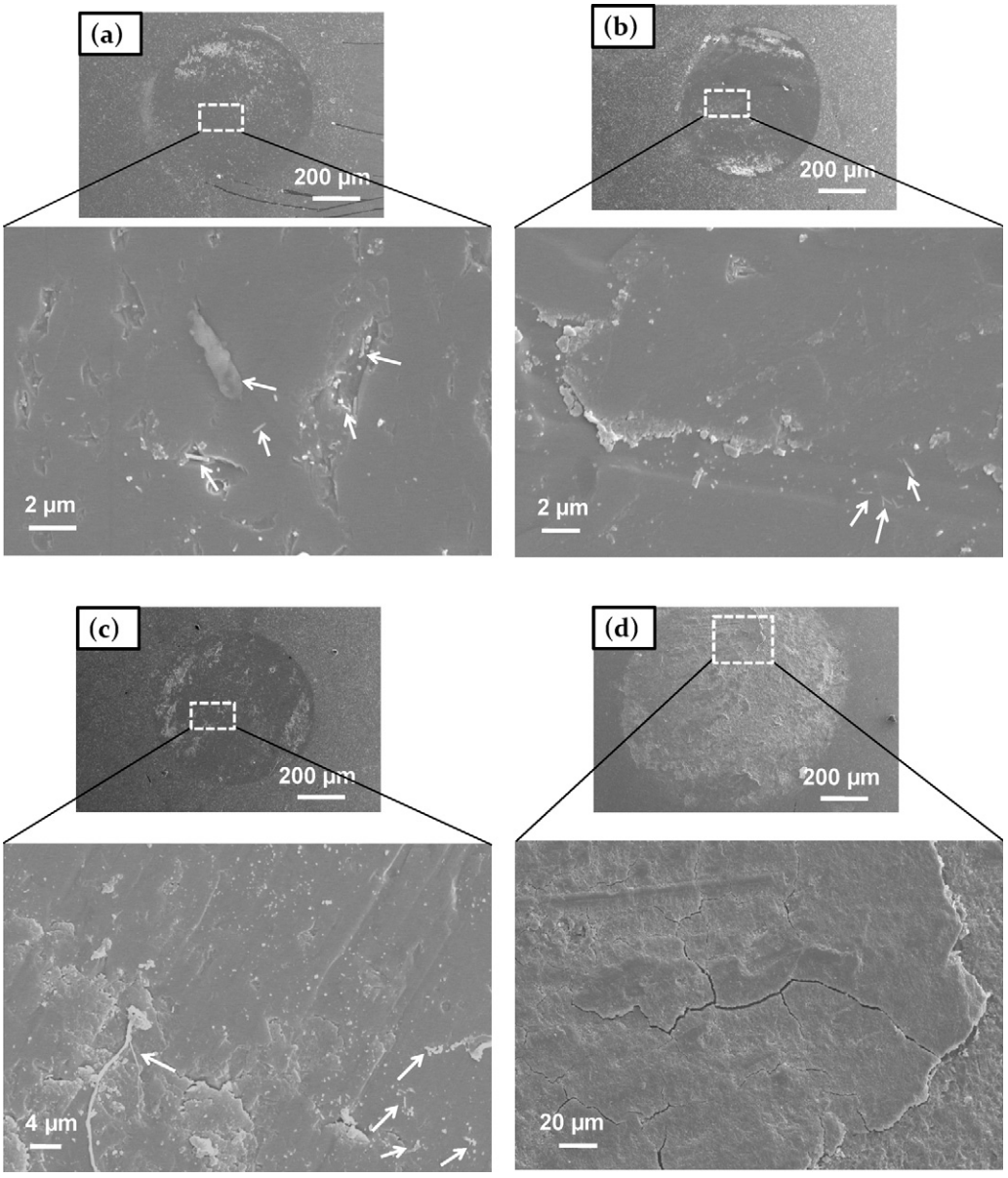

Fig. 10. Worn surface of balls after sliding against SiC ceramics: (a) SCY3 at 6 N, (b) SCSc3 at 6 N, (c) SCSc10 at 6 N, and (d) SCSc3 at 13 N load. Arrows indicate the needle-like debris particles.

ranging from submicrons to microns are often observed on the worn surfaces of balls and disks (indicated with arrows in Figs. 8–10). It is widely reported that at moderate and high humid environments, SiC ceramics are accompanied by the humidity-driven tribo-reactions to form a soft layer of hydroxilated silicon oxide [7,8,11,38]. The debris generated from the tribochemical layers tend to roll during sliding and achieve needle-like shapes [39–41]. As the present study was also conducted in laboratory air with a relative humidity of $50 \pm 10\%$, it is probable that the tribochemical reactions occurred at 6 and 13 N loads generate needle-like wear debris that could roll during sliding and contribute to the reduction in friction.

The evolution of material removal mechanisms of the investigated SiC ceramics can be discussed in terms of the effect of applied load. During unlubricated sliding wear of SiC, two processes, mechanical fracture and tribochemical reactions are believed to occur simultaneously and compete with each other [6,8,12]. At low loads, the wear of ceramics initially occurs via microfracture followed by fatigue during sliding [5,12,38]. SEM observation of the worn surfaces at 1 N load in the present study also indicates microfracture and surface grooving (Fig. 7). The fatigue plays an important role during sliding such that the crack propagation velocity is zero up to a threshold stress and increases rapidly with increasing stress [38]. Accordingly, the sliding distance up to which microfracture dominates the wear process decreases, and the fatigue-induced wear increases with increase in load, generating large amounts of debris at the interface [38]. The large amount of debris in the laboratory humid conditions favors the formation of tribochemical layer at the interface (Figs. 8 and 9). The stability of the tribochemical layer is significant as material

damage occurs by the delamination and spalling of tribolayer [11]. With further increase in load to 13 N, the increased fracture of the tribolayer caused high material loss (Fig. 6).

The influence of sintering additives can be regarded as not only as the densification aids but also primary elements for the tailoring of properties, since properties are influenced by the microstructure and the chemistry of grain boundary phase in the resulting ceramics [36]. The variation of composition of the small amount of sintering additives in the present study resulted in a variation in microstructural characteristics, which in turn influenced the wear behavior of the SiC ceramics. The microstructure of fine equi-axed and large platelet grains in SCSc3 resulted in better wear resistance. Further, the grain boundary phase is important in the sense that degradation reactions initiated at these points. It is possible that microcracks easily nucleate and propagate under the applied contact stress along weak amorphous grain boundaries, resulting in high material removal [42]. Accordingly, high wear was observed for SCY3 consisting of amorphous grain boundary phase when compared against SCSc3 consisting of clean grain boundaries. This effect was dominant in intermediate or high loading conditions, while wear occurred via surface grooving or sub-grain size failure (microfracture) under low load of 1 N where the grain boundary effect was minimal. Furthermore, the stability of the tribolayer at the interface often depends on the stress state of the material. The formation of secondary phases (such as Y–Si–O–C shown in Fig. 2a) during liquid phase sintering causes residual stresses upon cooling due to thermal expansion mismatch with SiC grains. The residual stresses induce cracks and contribute to the material loss of the ceramics during sliding [16]. The results from the present study suggest that high residual stresses might have generated for the SiC ceramics sintered with AlN–Y_2O_3 additives when compared against ceramics sintered with AlN–Sc_2O_3 additives. Large amount of additives favor the formation of large volume fractions of junction phases during sintering that enhances the residual stresses at the grain interface. This can attribute to the observed high wear for the SCSc10.

The mechanical properties of the ceramics, particularly hardness and fracture toughness influence the wear behavior. Results from the present study also indicate that the wear of SiC ceramics sintered with the small amount of sintering additives depend on hardness and fracture toughness. Based on the small difference in hardness between the disk surface and counterbody ball surface, the material damage during initial stages of sliding is minimal in case of SCSc3. Also, the propagation of stress-induced cracking during sliding can be effectively minimized for the SCSc3 containing high fracture toughness. On the other hand, SCY3 or SCSc10 specimens consisting of low hardness and fracture toughness contributed to their high wear (Fig. 3).

4. Conclusions

SiC ceramics with small amount (3 wt%) of AlN–Sc_2O_3 and AlN–Y_2O_3 additives were fabricated, and the influence of additive composition on the unlubricated sliding wear behavior was studied. The following are major conclusions:

(a) Small amount (3 wt%) of AlN–Sc_2O_3 or AlN–Y_2O_3 systems was sufficient to produce highly densified (>98%) SiC ceramics.
(b) SiC ceramics prepared with 3 wt% AlN–Y_2O_3 additives consisted of mostly large equi-axed grains with amorphous grain boundary phase of ~1.2 nm thickness, while SiC ceramics sintered with 3 wt% AlN–Sc_2O_3 additives showed duplex microstructure of elongated and fine equi-axed grains with clean grain boundary phase.
(c) The influence of additive composition on dry sliding friction behavior of SiC ceramics was minimal. The steady state COF decreased from 0.56 to 0.22 with increase in load from 1 to 13 N.
(d) Wear rate increased from 10^{-6} to 10^{-5} $mm^3/N{\cdot}m$ with load, and depended on the sintering additive composition. SiC ceramics sintered with 3 wt% AlN–Sc_2O_3 additives exhibited low wear at a given load.
(e) Surface grooving and microcracking occurred at low load (1 N), while tribochemical wear was dominant at 6 and 13 N loads for all the ceramics.

Acknowledgment

This research was supported by a grant from the Fundamental R&D Program for Technology of World Premier Materials funded by the Ministry of Knowledge Economy, Republic of Korea.

References

[1] F.F. Lange, Hot-pressing behaviour of silicon carbide powders with additions of aluminium oxide, J. Mater. Sci. 10 (1975) 314–320.
[2] N.P. Padture, *In situ*-toughened silicon carbide, J. Am. Ceram. Soc. 77 (1994) 519–523.
[3] G. Roewer1, U. Herzog, K. Trommer, E. Miiller, S. Friihauf, Silicon carbide—a survey of synthetic approaches, properties and applications, Struct. Bond. 101 (2002) 59–135.
[4] S.M. Hsu, M. Sheng, Wear prediction of ceramics, Wear 256 (2004) 867–878.
[5] X. Dong, S. Jahanmir, L.K. Ives, Wear transition diagram for silicon carbide, Tribo. Int. 28 (1995) 559–572.
[6] D.C. Cranmer, Friction and wear properties of monolithic silicon-based ceramics, J. Mater. Sci. 20 (1985) 2029–2037.
[7] K.H.Z. Gahr, R. Blattner, D.H. Hwang, K. Pohlmann, Micro and microtribological properties of SiC ceramics in sliding contact, Wear 250 (2001) 299–310.
[8] V.S.R. Murthy, H. Kobayashi, S. Tsurekawa, N. Tamari, T. Watanabe, K. Kato, Influence of humidity and doping elements on the friction and wear of SiC in unlubricated sliding, Tribo. Int. 37 (2004) 353–364.
[9] Y. Wang, S.M. Hsu, Wear and wear transition mechanisms of ceramics, Wear 195 (1996) 112–122.
[10] X.F. Zhang, G.Y. Lee, D. Chen, R.O. Ritchie, L.C.D. Jonghe, Abrasive wear behavior of heat-treated ABC-silicon carbide, J. Am. Ceram. Soc. 86 (2003) 1370–1378.
[11] P. Anderson, A. Blomberg, Instability in the tribochemical wear of silicon carbide in unlubricated sliding contacts, Wear 174 (1994) 1–7.
[12] O.O. Adewoye, T.F. Page, Frictional deformation and fracture in polycrystalline SiC and Si_3N_4, Wear 70 (1981) 37–51.

[13] S.J. Cho, C.D. Um, S.S. Kim, Wear and wear transition in silicon carbide ceramics during sliding, J. Am. Ceram. Soc. 79 (1996) 1247–1251.
[14] O.B. Lopez, A.L. Ortiz, F. Guiberteau, N.P. Padture, Sliding-wear-resistant liquid-phase-sintered SiC processed using α-SiC starting powders, J. Am. Ceram. Soc. 90 (2007) 541–545.
[15] O.B. Lopez, A.L. Ortiz, F. Guiberteau, N.P. Padture, Effect of microstructure on sliding-wear properties of liquid-phase-sintered α-SiC, J. Am. Ceram. Soc. 88 (2005) 2159–2163.
[16] O.B. Lopez, A.L. Ortiz, F. Guiberteau, N.P. Padture, Microstructural design of sliding-wear-resistant liquid-phase-sintered SiC: an overview, J. Eur. Ceram. Soc. 27 (2007) 3351–3357.
[17] D. Chen, X.F. Zhang, R.O. Ritchie, Effects of grain-boundary structure on the strength, toughness, and cyclic-fatigue properties of a monolithic silicon carbide, J. Am. Ceram. Soc. 83 (2000) 2079–2081.
[18] G. Rixecker, I. Wiedmann, A. Rosinus, F. Aldinger, High-temperature effect in the fracture mechanical behavior of silicon carbide liquid-phase sintered with AlN–Y_2O_3 additives, J. Eur. Ceram. Soc. 21 (2001) 1013–1019.
[19] S.G. Lee, Y.W. Kim, M. Mitomo, Relationship between microstructure and fracture toughness of toughened silicon carbide ceramics, J. Am. Ceram. Soc. 84 (2001) 1347–1353.
[20] R. Yuan, J.J. Kruzic, X.F. Zhang, L.C. De Jonghe, R.O. Ritchie, Ambient to high-temperature fracture toughness and cyclic fatigue behavior in Al-containing silicon carbide ceramics, Acta Mater. 51 (2003) 6477–6491.
[21] Y.W. Kim, M. Mitomo, T. Nishimura, High-temperature strength of liquid-phase-sintered SiC with AlN and RE_2O_3 (RE: Y, Yb), J. Am. Ceram. Soc. 85 (2002) 1007–1009.
[22] Y.W. Kim, M. Mitomo, T. Nishumura, Heat-resistant silicon carbide with aluminum nitride and erbium oxide, J. Am. Ceram. Soc. 84 (2001) 2060–2064.
[23] P.F. Becher, Microstructural design of toughened ceramics, J. Am. Ceram. Soc. 74 (1991) 255–269.
[24] H. Ye, G. Rixecker, S. Haug, F. Aldinger, Compositional identification of the intergranular phase in liquid phase sintered SiC, J. Eur. Ceram. Soc. 22 (2002) 2379–2387.
[25] K. Biswas, J. Schneider, G. Rixecker, F. Aldinger, Comparative bending creep behaviour of silicon carbide sintered with oxynitride additives, Scripta Mater. 53 (2005) 591–596.
[26] H.J. Choi, Y.W. Kim, M. Mitomo, T. Nishimura, J.H. Lee, D.Y. Kim, Intergranular glassy phase free SiC ceramics retains strength at 1500 °C, Scripta Mater. 50 (2004) 1203–1207.
[27] Y.W. Kim, S.H. Lee, T. Nishumura, M. Mitomo, Heat-resistant silicon carbide with aluminum nitride and scandium oxide, Acta Mater. 53 (2005) 4701–4708.
[28] Y.W. Kim, J.H. Lee, D.Y. Kim, Effect of sintering additive composition on grain boundary structure in liquid-phase-sintered silicon carbide, Mater. Sci. Forum 558–559 (2007) 897–902.
[29] Y.W. Kim, Y.S. Chun, T. Nishumura, M. Mitomo, Y.H. Lee, High-temperature strength of silicon carbide ceramics sintered with rare-earth oxide and aluminum nitride, Acta Mater. 55 (2007) 727–736.
[30] B.V.M. Kumar, M.H. Roh, Y.W. Kim, W. Kim, S.W. Park, W.S. Seo, Effect of additive composition on microstructure and mechanical properties of SiC ceramics sintered with small amount of RE_2O_3 (RE: Sc, Lu, Y) and AlN, J. Mater. Sci. 44 (2009) 5939–5943.
[31] G.R. Anstis, P. Chantikul, B.R. Lawn, D.B. Marshall, A critical evaluation of indentation techniques for measuring fracture toughness: I, direct crack measurements, J. Am. Ceram. Soc. 64 (1981) 533–538.
[32] D.S. Lim, J.W. An, H.J. Lee, Effect of carbon nanotube addition on the tribological behavior of carbon/carbon composites, Wear 252 (2002) 512–517.
[33] H.J. Choi, G.H. Kim, J.G. Lee, Y.W. Kim, Refined continuum model on the behavior of intergranular films in silicon nitride ceramics, J. Am. Ceram. Soc. 83 (2000) 2821–2827.
[34] G. Rixecker, K. Biswas, A. Rosinus, S. Sharma, I. Weidmann, F. Aldinger, Fracture properties of SiC ceramics with oxynitride additives, J. Eur. Ceram. Soc. 22 (2002) 2669–2675.
[35] N.P. Padture, B.R. Lawn, Toughness properties of a silicon carbide with an *in situ* induced heterogeneous grain structure, J. Am. Ceram. Soc. 77 (1994) 2518–2522.
[36] J.Y. Kim, Y.W. Kim, M. Mitomo, G.D. Zhan, J.G. Lee, Microstructure and mechanical properties of α-silicon carbide sintered with yttrium-aluminum garnet and silica, J. Am. Ceram. Soc. 82 (1999) 441–444.
[37] Y. Zhou, K. Hirao, Y. Yamauchi, S. Kanzaki, Tailoring the mechanical properties of silicon carbide ceramics by modification of the intergranular phase chemistry and microstructure, J. Eur. Ceram. Soc. 22 (2002) 2689–2696.
[38] T.E. Fischer, Z. Zhu, H. Kim, D.D. Shin, Genesis and role of wear debris in sliding wear of ceramics, Wear 245 (2000) 53–60.
[39] P. Anderson, J. Juhanko, A.P. Nikkila, P. Lintula, Influence of topography on the running-in of water-lubricated silicon carbide journal bearings, Wear 201 (1996) 1–9.
[40] T.E. Fischer, H. Tomizawa, Interaction of tribochemistry and microfracture in the friction and wear of silicon nitride, Wear 105 (1985) 29–45.
[41] M. Kalin, S. Jahanmir, G. Drazic, Wear mechanisms of glass-infiltrated alumina sliding against alumina in water, J. Am. Ceram. Soc. 88 (2005) 346–352.
[42] A. Krell, P. Blank, Inherent reinforcement of ceramic microstructure by grain boundary engineering, J. Eur. Ceram. Soc. 9 (1992) 309–322.